Development and performance verification of a TPC polarimeter for high energy x-rays

Takeda, Tomoshi, Black, Kevin, Enoto, Teruaki, Hayato, Asami, Hill, Joanne, et al.

Tomoshi Takeda, Kevin Black, Teruaki Enoto, Asami Hayato, Joanne Hill, Wataru Iwakiri, Keith Jahoda, Takao Kitaguchi, Miho Okubo, Toru Tamagawa, Marina Tsutsumi, Keisuke Uchiyama, Yuto Yoshida, Yuanhui Zhou, "Development and performance verification of a TPC polarimeter for high energy x-rays," Proc. SPIE 11444, Space Telescopes and Instrumentation 2020: Ultraviolet to Gamma Ray, 114445Y (13 December 2020); doi: 10.1117/12.2561313

SPIE.

Event: SPIE Astronomical Telescopes + Instrumentation, 2020, Online Only

Development and performance verification of a TPC polarimeter for high energy X-rays

Tomoshi Takeda[a,b], Kevin Black[c,d], Teruaki Enoto[e], Asami Hayato[f], Joanne Hill[c], Wataru Iwakiri[g], Keith Jahoda[c], Takao Kitaguchi[e], Miho Okubo[a], Toru Tamagawa[a,e], Marina Tsutsumi[a], Keisuke Uchiyama[a], Yuto Yoshida[a], and Yuanhui Zhou[a]

[a]RIKEN Nishina Center, 2-1 Hirosawa, Wako, Saitama, 351-0198, Japan
[b]Department of Physics, Tokyo University of Science, 1-3 Kagurazaka, Shinjyuku-ku,, Tokyo 162-8601, Japan
[c]NASA Goddard Space Flight Center, Greenbelt, MD 20771, USA
[d]Rock Creek Scientific, 1400 East-West Hwy, Silver Spring, MD, 20910, USA
[e]RIKEN Cluster for Pioneering Research, 2-1 Hirosawa, Wako, Saitama 351-0198, Japan
[f]JAXA Tsukuba Space Center, 2-1-1 Sengen, Tsukuba, Ibaraki 305-8505, Japan
[g]Department of Physics, Faculty of Science and Engineering, Chuo University, 1-13-27 Kasuga, Bunkyo-ku, Tokyo 112-8551, Japan

ABSTRACT

We present the first application of a time projection chamber polarimeter to measure high energy X-ray polarization above 10 keV. The polarimeter is designed based on the PRAXyS soft X-ray polarimeter. The sealed gas is changed to a gas mixture of 60% argon and 40% dimethyl ether at 1 atm to be sensitive to high energy X-rays. The polarimeter performance is verified with linearly polarized, monochromatic X-rays at a synchrotron radiation facility, KEK Photon Factory BL-14A. The measured modulation factors are $42.4 \pm 0.6\%$, $50.4 \pm 0.6\%$, and $55.0 \pm 0.6\%$ at 12, 14, and 16 keV, respectively, and the measured polarization angles are consistent with the expected values at all energies.

Keywords: X-ray astronomy, polarimetry, photoelectric polarimeter, Time Projection Chamber (TPC)

1. INTRODUCTION

Cosmic X-ray polarimetry is expected to play a crucial role in astrophysics because it can provide information independently of other observation methods: imaging, timing, and spectroscopy. However, due to the difficulty in developing a highly sensitive X-ray polarimeter, X-ray polarization has not been sufficiently exploited except for the detection of Crab Nebulae in the 1970s.[1] Ideally, polarization sensitivity is desired across a broad energy band to understand the comprehensive physical nature of a target. Photoelectric and Compton scattering polarimeters are suitable for the soft and hard X-ray bands, respectively, because each is the most dominant photon interaction in the respective energy band. Soft X-ray polarimetry in the energy band of 2–8 keV will be opened up by the photoelectric polarimeters on-board the Imaging X-ray Polarimetry Explorer (IXPE), NASA's Small Explorer (SMEX) satellite mission to be launched in 2021.[2] On the other hand, the hard X-ray band above 20 keV has been explored by balloon experiments equipped with a Compton polarimeter such as X-Calibur[3] and *PoGO+*.[4] X-ray polarimetry in the energy range of 8–20 keV is essential because non-thermal radiation from a celestial object dominates thermal radiation, expecting a high polarization degree with enough photon statistics. However, there is still no polarimeter dedicated to this band, where the cross sections of the photoelectric absorption and Compton scattering are comparable. In this paper, we report the detector performance of a photoelectric polarimeter with a time projection chamber (TPC) technique[5] developed to measure high energy X-ray polarization above 10 keV.

Further author information: (Send correspondence to Tomoshi Takeda)
Tomoshi Takeda: E-mail: tomoshi.takeda@riken.jp

Space Telescopes and Instrumentation 2020: Ultraviolet to Gamma Ray, edited by Jan-Willem A. den Herder
Shouleh Nikzad, Kazuhiro Nakazawa, Proc. of SPIE Vol. 11444, 114445Y · © 2020 SPIE
CCC code: 0277-786X/20/$21 · doi: 10.1117/12.2561313

Photoelectric polarimeter can detect X-ray polarization by utilizing the intrinsic nature that the angular distribution of photoelectron emission is sensitive to the polarization direction of incident X-rays. The emission angle of the K-shell photoelectron projected onto a plane perpendicular to the incident direction follows the probability distribution, $\cos^2(\phi - \phi_0)$, where ϕ and ϕ_0 are the azimuth angle of emitted photoelectron and the polarization direction of the incident photon, respectively. A histogram of emission angles is commonly known as the "modulation curve." The modulation curve without a systematic modulation due to detector effects follows the distribution

$$N(\phi) = C\left(1 + \frac{M}{100}\cos 2(\phi - \phi_0)\right), \tag{1}$$

where C is the constant and M is the modulation amplitude in %. The detector analyzing power of the polarization, modulation factor μ, is defined as modulation amplitude M for 100% polarized X-rays. When the polarization degree of the calibration source is M_c, the modulation factor is given by M/M_c.

The gas pixel detector (GPD[6]) and the TPC polarimeter are two representative types of the photoelectric polarimeter. In the GPD, the photoelectron tracks drift parallel to the optical axis, making it possible to image the celestial objects, but it is difficult to achieve high quantum efficiency (QE) because the detector depth cannot be increased due to the electron diffusion, which blurs the track and deteriorates the modulation factor. By contrast, in the TPC polarimeter, because the direction of the electron drift is perpendicular to the optical axis, it is not capable of imaging, but instead, the detector depth can be increased without increasing the electron diffusion effect, resulting in high QE. We previously developed the TPC polarimeter for the Polarimeter for Relativistic Astrophysical X-ray Sources (PRAXyS) mission filled with dimethyl ether (DME) at 0.25 atm and covering the soft X-ray band (2–10 keV).[7] Here we demonstrate the performance of a TPC polarimeter modified for high energy X-rays above 10 keV.

2. EXPERIMENTAL SETUP

2.1 TPC Polarimeter for High Energy X-rays

To select the appropriate gas for the energy range of interest, the QE, electron diffusion, and drift velocity, as well as the K-shell binding energy, are considered. Furthermore, the energy of an Auger electron is required to be low to avoid confusing the photoelectron track. DME gas has a relatively slow drift velocity and K-shell binding energy suitable for a photoelectric polarimeter below the observed energy band of 10 keV. However, to have sufficient QE above 10 keV requires DME gas pressure greater than 2 atm, where there is a risk of breaking the 100 μm-thick beryllium window of our polarimeter originally developed for measuring soft X-ray polarization. Although xenon gas is widely used for higher energy X-ray detectors and has much higher QE, its K-shell binding energy of 34.6 keV is too high for the energy range of interest. Adopting a high-Z gas, such as argon with K-shell binding energy of 3.2 keV, has sufficient QE at pressures where the photoelectron path length is long enough to measure the emission angle. For this demonstration, we employ a gas mixture of argon 60% and DME 40% at a pressure of 1 atm.

Figure 1 (a) shows the schematic view of the experimental setup. The polarimeter consists of a drift electrode, field cage, a gas electron multiplier (GEM[8,9]), 128-ch readout strips, and readout electronics. The effective depth along the optical axis is 7.8 cm. The height between the drift electrode and the GEM is 1.95 cm, and the gap between the GEM and the readout strips (transfer gap) is 0.2 mm. The GEM has a thickness of 100 μm, an active area of 7.8×3 cm^2, and a hole diameter and pitch of 70 and 121 μm, respectively. These devices are installed in a chamber made of aluminum. The chamber is cylindrical, whose diameter and length are approximately 20 cm and 30 cm, respectively. Assuming the same four units are placed along the optical axis in the chamber, which is the same design as the PRAXyS polarimeter, the QE is expected to be 72% at 10 keV.

The main difference with the PRAXyS polarimeter is the signal readout system. We employ the Scalable Readout System (SRS[10]) developed by the CERN/RD51 collaboration. Ref. 11 demonstrated that the performance of the TPC polarimeter combined with the SRS is comparable to that of the PRAXyS polarimeter. In addition, the polarimeter can be rotated around the cylinder axis as shown in Figure 1 (b), allowing us to obtain unpolarized data by adding two modulation curves for polarized X-rays measured at 90 degrees different angles.

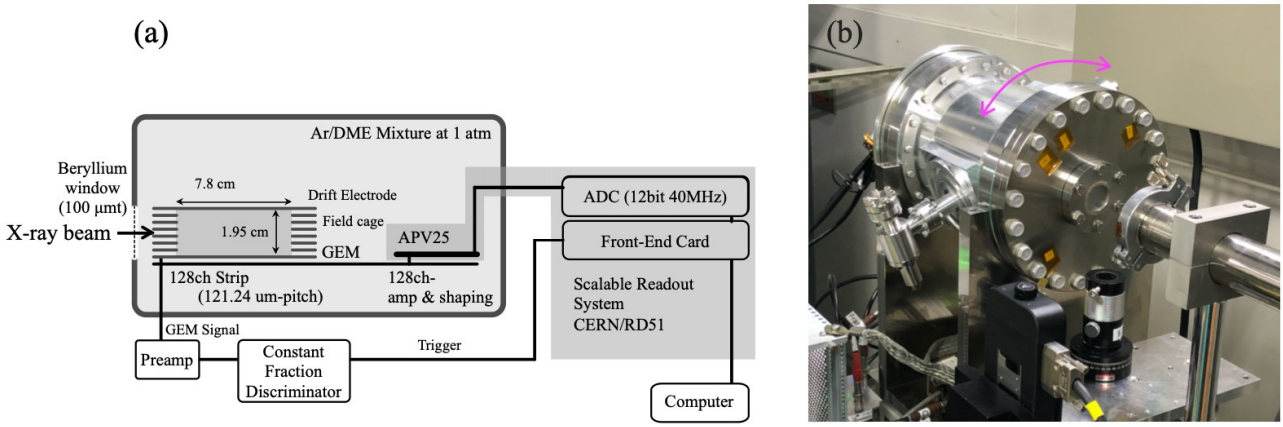

Figure 1. (a) Schematic view of the experimental setup. Incident X-rays enter the detector through a beryllium window, and the electron signal is read out via the SRS/APV25 readout system, whose trigger is generated by the GEM cathode signal. (b) Appearance of the TPC polarimeter. The chamber is made of aluminum, has a cylindrical shape, and can be easily rotated around the axis.

The electron signals from the strips are read out via the APV25 ASIC,[12] which has 128 channels, each with a charge sensitive preamplifier and shaping amplifier with a nominal time constant of 50 ns. The signals are then continuously digitized by an ADC at a sampling rate of 40 MHz. An external trigger for the readout is generated by the GEM cathode signal, processed through a constant fraction discriminator (ORTEC 583) to suppress a dependence of the trigger timing on pulse heights. A 2-D image is obtained with the TPC technique applied to the 1-D strips readout. In order to square pixels in the 2-D image, the electron drift velocity must be set to 4.85 cm μs^{-1}, where the drift velocity multiplied by the sampling duration (25 ns) is equal to the strip spacing (121 μm). After calibrating the drift velocity with a modulated X-ray source (MXS[13]), the drift field was set to be 601 V cm^{-1}. The transfer field between the GEM anode and strips was set at 2500 V cm^{-1} to maximize the collection efficiency of electrons. Figure 2 shows the effective gain as a function of the applied voltage to the GEM. The applied voltage was set at 630 V, where the effective gain is approximately 1350.

2.2 Performance verification with Synchrotron X-rays

We carried out the performance verification of the polarimeter with linearly polarized, monochromatic X-rays at a synchrotron radiation facility, KEK Photon Factory BL-14A. The polarimeter was irradiated with monochromatic X-rays at three different energies of 12, 14, and 16 keV. The X-ray beam was collimated to a 60 μm square, and its height was 2.7 mm above the GEM. We took data at two different detector inclination: the angle between the electron drift direction and the beam polarization direction was +45 and -45 deg. We recorded 15×10^4 events at each energy and each inclination angle to collect polarized data. In addition, we recorded 7.5×10^4 events to create unpolarized data by adding two data sets which are at right inclination angles to each other. Figure 3 shows the measured ADC spectra. The energy resolutions in FWHM are 16.0, 14.0, and 13.3% at 12, 14, and 16 keV, respectively.

In order to measure the polarization degree of the synchrotron X-ray beam, we used the Compton scattering polarimeter consists of cylindrical Be scatterer and Amptek Si detector placed perpendicular to the optical axis. Because perpendicularly scattered X-rays are extracted and counted by the Si detector, the Compton polarimeter has a very low QE but a high modulation factor more than 90% and is therefore suitable to measure the polarization degree with high accuracy. The measured beam polarization degrees are $82.1 \pm 0.1, 80.6 \pm 0.2$, and $80.3 \pm 0.2\%$ at 12, 14, and 16 keV, respectively. These values are consistent with the results previously presented in Ref. 14.

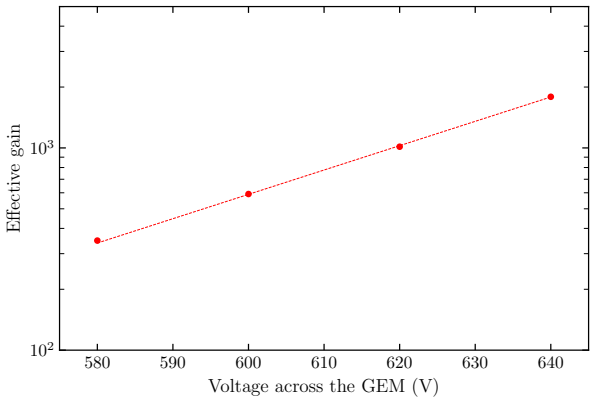

Figure 2. Effective gain as a function of the applied voltage to the GEM in the gas mixture of argon 60% and DME 40% at 1 atm. The dashed line is the best-fit exponential model.

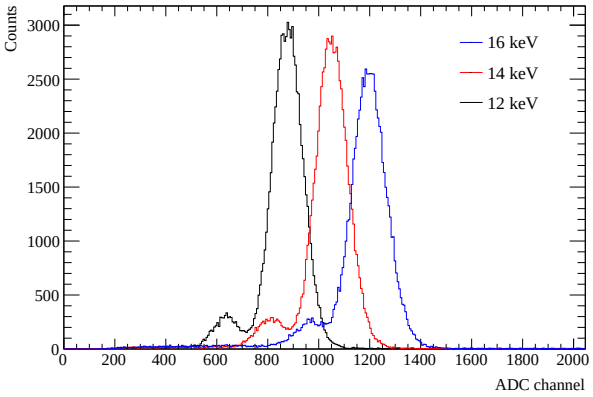

Figure 3. ADC spectra measured at the GEM cathode at different energies of 12 keV (black), 14 keV (red), and 16 keV (blue). The sub peak of each spectrum corresponds to the argon escape peak.

3. DATA ANALYSIS

3.1 Data Processing

The following image processing procedure is based on Ref. 7. A raw track image taken with the TPC technique is elongated along the time direction due to the signal shaping with a time constant of 50 ns. The raw image is deconvolved with the shaper response, which is obtained by using an internal test pulse generated in the APV25 ASIC. Furthermore, Gaussian convolution along the time direction is performed to correct for diffusion asymmetry in the transfer gap. The Gaussian sigma is set to be 83.0 μm so that the measured polarization angles are consistent with the expected angles in our test configuration. Only pixels with a charge greater than 3 times the root mean square noise are included in the following analysis.

3.2 Angular Reconstruction

We employ angular reconstruction with image moments to determine the initial emission angle of the photoelectron. The method derives image orientation from the major principal axis with respect to the charge centroid. However, in the higher energy range, a long track is curved due to Coulomb scattering. In order to cut the curved track and leave the initial part, we use the adaptive cut method described in Ref. 15. The method controls the track image by cutting with the threshold of the number of hit pixels, μ'_{00}, and the maximum second moment with respect to the charge centroid, $M_2^{\max}$. The track image is repeatedly cut off in a 0.5-pixel step along the major axis from the Bragg peak at the endpoint of the track until either μ'_{00} or $M_2^{\max}$ of the remaining track falls below the thresholds.

The threshold of μ'_{00} is set to avoid overcutting short tracks in the lower energy range, where the diffusion size which blurs the image is greater than the photoelectron track length. The threshold of μ'_{00} should be as small as possible within the range where tracks are not excessively cut, because if this value is large, another threshold, $M_2^{\max}$, in the higher energy range becomes useless. To determine the optimal value, we used the 8.0 keV line produced by an X-ray generator with copper as an anode target. The typical photoelectron range induced by an 8.0 keV X-ray is approximately 0.4 mm, or 3 pixels, based on the calculation with the semi-empirical equation in Ref. 16. We optimized these two thresholds with the grid search to maximize the total modulation amplitude of the 12, 14, and 16 keV polarized data sets and minimize a fake modulation amplitude of the unpolarized 8 keV data. As a result, the optimal threshold condition is found as follows,

$$(\mu'_{00} \leq 23) \text{ or } (M_2^{\max} \leq 1.6). \tag{2}$$

Track images in Figure 4 show that the major principal axis of the remaining track after cutting the curved part with the above method is a good estimator of the initial emission angle of photoelectrons.

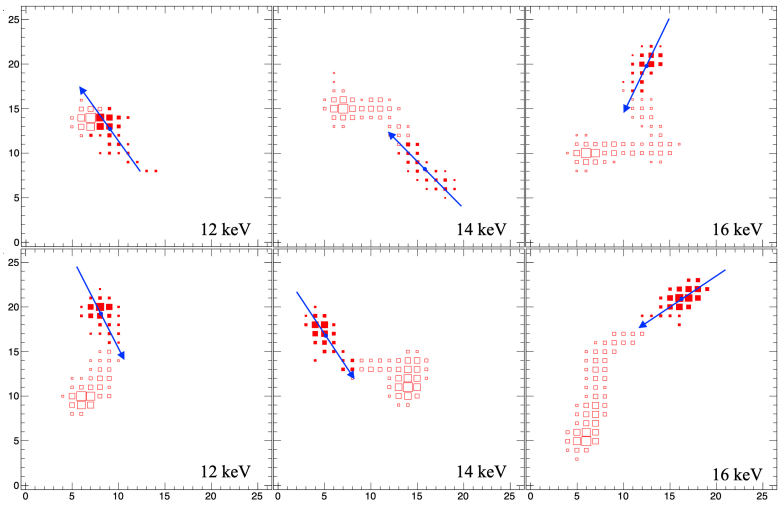

Figure 4. Example of photoelectron track images with predicted angles of the initial emission. The size of the box corresponds to the amount of charge detected in each pixel. The arrows indicate predicted angles of the initial emission using the adaptive cut method. Only the filled boxes are used to calculate the image moments.

4. POLARIMETER PERFORMANCE

The modulation curves for unpolarized X-rays are created by adding the two modulation curves measured at 90 deg different detector inclinations: +45 and -45 deg. Although the unpolarized curve is not flat due to unoptimized detector settings (see Appendix A for details), it can be canceled out by dividing a polarized curve by the unpolarized one. Figure 5 shows the corrected modulation curves for -45 deg detector inclination. The results of fitting the sinusoidal model in Eq. 1 to the corrected modulation curves show that the measured modulation amplitudes are $35.0 \pm 0.5\%$, $40.9 \pm 0.5\%$, and $44.8 \pm 0.5\%$ at 12, 14, and 16 keV, respectively. Combining the modulation amplitudes with the measured beam polarization degrees described in Section 2.2, the modulation factors are calculated to be $42.7 \pm 0.9\%$, $50.7 \pm 0.9\%$, and $55.8 \pm 0.9\%$ at 12, 14, and 16 keV, respectively. The measured polarization angles are consistent with the expected values at all energies. The fit results and the modulation factors for all the data are summarized in Table 1. The average modulation factors of the ± 45 deg data sets are $42.4 \pm 0.6\%$, $50.4 \pm 0.6\%$, and $55.0 \pm 0.6\%$ at 12, 14, and 16 keV, respectively. The measured polarization angles are consistent with the data sets at all energies. The modulation factors measured here are comparable to the X-Calibur Compton polarimeter with a modulation factor of $\sim$50%.[3] Optimization of the gas mixture and a more sophisticated data processing algorithm[17] can improve the polarimeter performance. Therefore, the TPC polarimeter is efficient to detect not only soft X-rays (2–10 keV) but also hard X-rays above 10 keV.

Table 1. Best-fit parameters for the corrected modulation curves and derived modulation factors. All errors correspond to the 1σ confidence level.

Energy (keV)	Detector inclination (deg)	ϕ_0 (deg)	M (%)	μ (%)	χ^2/d.o.f
12	+45	46.3 ± 0.4	34.4 ± 0.5	42.0 ± 0.9	43.41/57
	−45	-44.5 ± 0.4	35.0 ± 0.5	42.7 ± 0.9	67.00/57
14	+45	46.3 ± 0.4	40.3 ± 0.5	50.0 ± 0.9	50.44/57
	−45	-44.8 ± 0.4	40.9 ± 0.5	50.7 ± 0.9	58.85/57
16	+45	44.8 ± 0.3	43.5 ± 0.5	54.2 ± 0.9	39.76/57
	−45	-45.2 ± 0.5	44.8 ± 0.5	55.8 ± 0.9	61.15/57

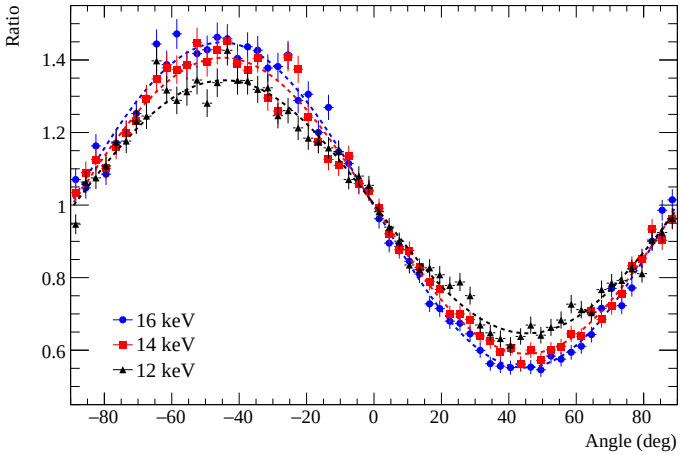

Figure 5. Corrected modulation curves created by dividing the polarized modulation curves by the unpolarized ones. The dashed lines are the best-fit sinusoidal models.

5. SUMMARY

In this work, we present the first application of a TPC polarimeter to measure high energy X-ray polarization above 10 keV. The performance verification was carried out at a synchrotron radiation facility, KEK Photon Factory BL-14A. The experimental results are summarized below.

1. The measured energy resolutions (FWHM) are 16.0, 14.0, and 13.3% at 12, 14, and 16 keV, respectively.
2. The measured modulation factors are $42.4 \pm 0.6\%$, $50.4 \pm 0.6\%$, and $55.0 \pm 0.6\%$ at 12, 14, and 16 keV, respectively.
3. The reconstructed polarization angles are consistent with the expected values at all energies.

APPENDIX A. REDUCTION OF A FALSE MODULATION

Although the PRAXyS soft X-ray polarimeter showed no significant false modulation for unpolarized X-rays,[7] the unpolarized modulation curve measured with the developed polarimeter has the false modulation as described in Section 4. In order to reduce it, we optimize the detector setting with an X-ray generator. Figure 6 shows the energy spectrum of X-rays from the X-ray generator with an electron accelerating voltage of 20 kV and target material of copper. The X-ray beam is collimated to a 200 μm square size using a collimator. The low energy X-rays below 10 keV are reduced by a 312 μm-thick aluminum filter. Since bremsstrahlung X-rays, which are the main continuum radiation of the X-ray generator, are partially polarized,[18] we add two modulation curves whose detector inclination angles are perpendicular to each other to create unpolarized data in the same way as described in Section 4. We set the same detector parameters as the performance verification experiment with synchrotron X-rays and obtain the 12–14 keV modulation curve for unpolarized data shown in Figure 7 (a). The false modulation is also found in X-rays from the X-ray generator. Its amplitude is 13.5% derived from the maximum and minimum counts.

We find that a nonlinear gain of the APV25 preamplifier produces the false modulation. Compared to the PRAXyS soft X-ray polarimeter, a charge amount measured with the developed polarimeter increases by a factor of a few due to the higher X-ray energy. Therefore, some of the signals are preamplified in the nonlinear (or nearly saturated) region, resulting in track image distortion along the time direction. We reduce the GEM gain from 1350 to 700 to operate the APV25 preamplifier in the linear gain region and obtain the modulation curves shown in Figure 7 (b). The false modulation amplitude for the unpolarized data is $0.33 \pm 0.38\%$, calculated by fitting the sinusoidal model to the curve, showing that the polarimeter developed for high energy X-rays can be set to have no significant false modulation.

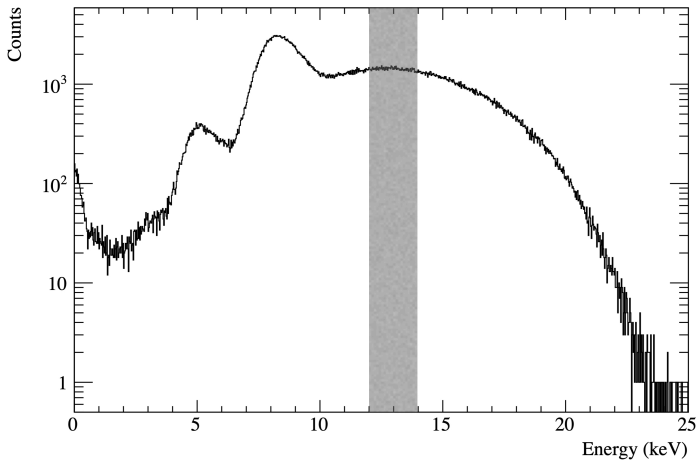

Figure 6. Energy spectra of X-rays generated with the X-ray generator. The anode target is copper and the applied tube voltage is 20 kV. The shaded box indicates the energy range in which events are extracted for the analysis.

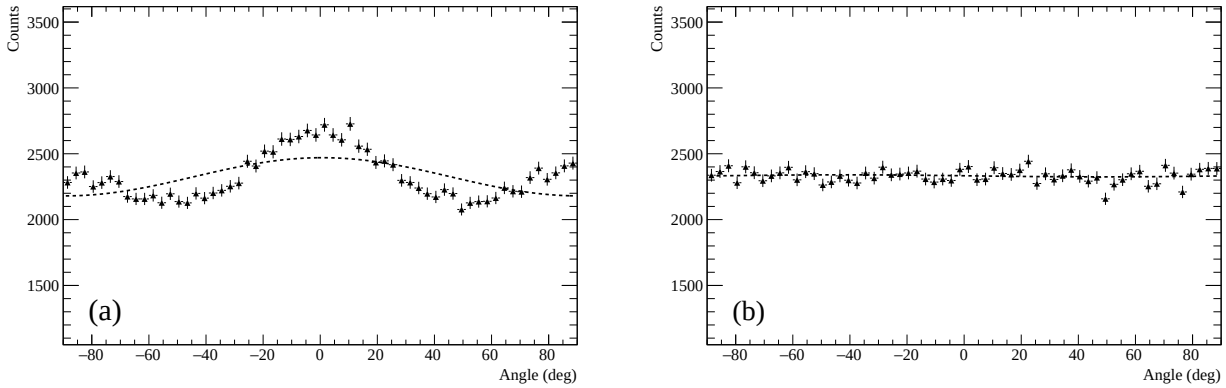

Figure 7. Comparison of modulation curve for unpolarized X-ray (a) before and (b) after the adjustment. The dashed lines are the best-fit sinusoidal models.

ACKNOWLEDGMENTS

The detector calibration with synchrotron X-rays was performed at the BL-14A of KEK Photon Factory under the approval of the Photon Factory Program Advisory Committee (Proposal No.2019G044). The authors would like to thank Dr. Shunji Kishimoto for his help on the beamline adjustment. A. Hayato was supported by Research Fellow of Japan Society for the Promotion of Science, 17J40001. This work was partially supported by the research grant from Research Foundation for Opto-Science and Technology and JSPS KAKENHI Grant Number JP16H02198.

REFERENCES

[1] Weisskopf, M., Silver, E., Kestenbaum, H., Long, K., and Novick, R., "A precision measurement of the x-ray polarization of the crab nebula without pulsar contamination," *The Astrophysical Journal* **220** (1978).

[2] Weisskopf, M. C., Ramsey, B., O'Dell, S. L., Tennant, A., Elsner, R., Soffita, P., Bellazzini, R., Costa, E., Kolodziejczak, J., Kaspi, V., Mulieri, F., Marshall, H., Matt, G., and Romani, R., "The Imaging X-ray Polarimetry Explorer (IXPE)," *Results in Physics* **6**, 1179–1180 (2016).

[3] Beilicke, M., Kislat, F., Zajczyk, A., Guo, Q., Endsley, R., Stork, M., Cowsik, R., Dowkontt, P., Barthelmy, S., Hams, T., Okajima, T., Sasaki, M., Zeiger, B., De Geronimo, G., Baring, M. G., and Krawczynski, H., "Design and Performance of the X-ray Polarimeter X-Calibur," *Journal of Astronomical Instrumentation* **3**(2), 1–47 (2014).

[4] Chauvin, M., Florén, H.-G., Friis, M., Jackson, M., Kamae, T., Kataoka, J., Kawano, T., Kiss, M., Mikhalev, V., Mizuno, T., Tajima, H., Takahashi, H., Uchida, N., and Pearce, M., "The pogo+ view on crab off-pulse hard x-ray polarization," *Monthly Notices of the Royal Astronomical Society: Letters* **477**(1), L45–L49 (2018).

[5] Black, J. K., Baker, R. G., Deines-Jones, P., Hill, J. E., and Jahoda, K., "X-ray polarimetry with a micropattern TPC," *Nuclear Instruments and Methods in Physics Research, Section A: Accelerators, Spectrometers, Detectors and Associated Equipment* **581**(3), 755–760 (2007).

[6] Costa, E., Soffitta, P., Bellazzini, R., Brez, A., Lumb, N., and Spandre, G., "An efficient photoelectric X-ray polarimeter for the study of black holes and neutron stars," *Nature* **411**(6838), 662–665 (2001).

[7] Iwakiri, W. B., Black, J. K., Cole, R., Enoto, T., Hayato, A., Hill, J. E., Jahoda, K., Kaaret, P., Kitaguchi, T., Kubota, M., Marlowe, H., Mccurdy, R., Takeuchi, Y., and Tamagawa, T., "Performance of the PRAXyS X-ray polarimeter," *Nuclear Instruments and Methods in Physics Research, Section A: Accelerators, Spectrometers, Detectors and Associated Equipment* **838**, 89–95 (2016).

[8] Sauli, F., "GEM : A new conce pt for electron a mplification in gas detectors," *Nuclear Instruments and Methods in Physics Research, Section A: Accelerators, Spectrometers, Detectors and Associated Equipment* **386**(96) (1997).

[9] Tamagawa, T., Hayato, A., Asami, F., Abe, K., Iwamoto, S., Nakamura, S., Harayama, A., Iwahashi, T., Konami, S., Hamagaki, H., Yamaguchi, Y. L., Tawara, H., and Makishima, K., "Development of thick-foil and fine-pitch GEMs with a laser etching technique," *Nuclear Instruments and Methods in Physics Research, Section A: Accelerators, Spectrometers, Detectors and Associated Equipment* **608**(3), 390–396 (2009).

[10] Martoiu, S., Muller, H., Tarazona, A., and Toledo, J., "Development of the scalable readout system for micro-pattern gas detectors and other applications," *Journal of Instrumentation* **8**(3) (2013).

[11] Kitaguchi, T., Hayato, A., Iwakiri, W., Takeuchi, Y., Kubota, M., Nishida, K., Enoto, T., and Tamagawa, T., "Development of the GEM-TPC X-ray polarimeter with the scalable readout system," *EPJ Web of Conferences* **174**, 2016–2019 (2018).

[12] French, M. et al., "Design and results from the APV25, a deep sub-micron CMOS front-end chip for the CMS tracker," *Nucl. Instrum. Meth. A* **466**, 359–365 (2001).

[13] Gendreau, K., Arzoumanian, Z., Asami, F., Baker, R., Balsamo, E., Black, K., Duran-Aviles, C., Enoto, T., Gregory, K., Hahne, D., Hayato, A., Hill, J., Huegel, F., Iwahashi, T., Iwakiri, W., Jahoda, K., Jalota, L., Kaaret, P., Kaneko, K., Kenyon, S., Kitaguchi, T., Koenecke, R., Kohmura, T., Okajima, T., Olsen, L., Porter, F. S., Rush, K., Serlemitsos, P., Soong, Y., Takeuchi, Y., Tamagawa, T., Yamada, S., and Yoshikawa, A., "The x-ray advanced concepts testbed (XACT) sounding rocket payload," in [*Space Telescopes and Instrumentation 2012: Ultraviolet to Gamma Ray*], Takahashi, T., Murray, S. S., and den Herder, J.-W. A., eds., **8443**, 1408 – 1414, International Society for Optics and Photonics, SPIE (2012).

[14] Tokanai, F., Sakurai, H., Gunji, S., Motegi, S., Toyokawa, H., Suzuki, M., Hirota, K., Kishimoto, S., and Hayashida, K., "Hard X-ray polarization measured with a Compton polarimeter at synchrotron radiation facility," *Nuclear Instruments and Methods in Physics Research, Section A: Accelerators, Spectrometers, Detectors and Associated Equipment* **530**(3), 446–452 (2004).

[15] Kitaguchi, T., Black, K., Enoto, T., Fukazawa, Y., Hayato, A., Hill, J. E., Iwakiri, W. B., Jahoda, K., Kaaret, P., McCurdy, R., Mizuno, T., Nakano, T., and Tamagawa, T., "An optimized photoelectron track reconstruction method for photoelectric X-ray polarimeters," *Nuclear Instruments and Methods in Physics Research, Section A: Accelerators, Spectrometers, Detectors and Associated Equipment* **880**(May 2017), 188–193 (2018).

[16] Tabata, T., Ito, R., and Okabe, S., "Generalized semiempirical equations for the extrapolated range of electrons," *Nuclear Instruments and Methods* **103**(1), 85 – 91 (1972).

[17] Kitaguchi, T., Black, K., Enoto, T., Hayato, A., Hill, J. E., Iwakiri, W. B., Kaaret, P., Mizuno, T., and Tamagawa, T., "A convolutional neural network approach for reconstructing polarization information of photoelectric X-ray polarimeters," *Nuclear Instruments and Methods in Physics Research, Section A: Accelerators, Spectrometers, Detectors and Associated Equipment* **942**, 1–24 (2019).

[18] Tanaka, S., Tsunemi, H., and Hayashida, K., "How linearly polarized is the X-ray beam from the X-ray generator?," *Japanese Journal of Applied Physics, Part 1: Regular Papers and Short Notes and Review Papers* **36**(9 A), 5770–5773 (1997).